HHS Public Access

Author manuscript

Aerosol Sci Technol. Author manuscript; available in PMC 2017 September 02.

Published in final edited form as:

Aerosol Sci Technol. 2016 ; 50(11): 1167–1179. doi:10.1080/02786826.2016.1230662.

Miniature Differential Mobility Analyzer for Compact Field-Portable Spectrometers

Chaolong Qi and **Pramod Kulkarni***

Centers for Disease Control and Prevention, National Institute for Occupational Safety and Health, 1090 Tusculum Ave, MS: R7, Cincinnati, OH, 45226

Abstract

A low-flow miniature differential mobility analyzer (mDMA) has been developed for compact field-portable mobility spectrometers to classify the submicrometer aerosol. The mDMA was designed for an ultra-low aerosol flow rate of 0.05 L/min. At a sheath flow rate of 0.2 L/min, the mDMA's upper size limit was estimated to be about 921 nm. The mDMA has a classification zone of 2.54 cm long, an outer diameter of 2.54 cm, and an inner diameter of 1.778 cm. The design allows low-cost fabrication and easy assembly. Tandem DMA (TDMA) measurements were carried out to evaluate the performance of the mDMA. Its transfer function was described using Stolzenburg's model. The experimentally measured transfer function shows close agreement with the theory. The transmission efficiency was comparable to that of the Knutson-Whitby DMA for particles in the range of 10–1000 nm. The mobility resolution was comparable to that of the TSI 3085 nanoDMA at the same aerosol flow rate. The design features and performance of the mDMA make it suitable for compact field portable mobility size spectrometers for measurement of nanoparticles and submicrometer aerosol.

1. Introduction

Measurement of aerosol size distribution is critical for understanding the impact of aerosols on human health and the global climate. Electrical mobility techniques have been widely used for size measurement of ultrafine aerosol, nanoparticles, and submicrometer aerosols due to their unique advantages over inertial or optical techniques. The differential mobility analyzers (DMA) have served a critical role in aerosol science, allowing separation of particles based on their electrical mobility. Since their initial development (Knutson and Whitby 1975; Liu and Pui 1975), DMAs have been extensively used for producing calibration aerosol and size classification and measurement. Several different designs of DMAs have been developed to overcome certain limitations of earlier designs, such as the Vienna type (Winklmayr et al. 1991), the French radial type (Fissan et al. 1998; Mesbah 1994), the Caltech radial type (Brunelli et al. 2009; Zhang et al. 1995), and the nanoDMA (Chen et al. 1998). Some other designs have also been developed to target specific size

*Corresponding Author: Pramod Kulkarni; Phone: (513) 841-4300, fax: (513) 841-4545, PSKulkarni@cdc.gov.

distribution measurement applications (Birmili et al. 1999; Li et al. 2009; Mei et al. 2011; Qi and Kulkarni 2012).

Growing concerns over inhalation exposure to nanoparticles have prompted development of compact instruments to characterize personal exposures in industrial atmospheres. In turn, such compact, portable instruments require design of smaller and efficient DMAs (Li et al. 2009; Qi and Kulkarni 2012). Most mobility spectrometers in use today employ DMAs that were not designed for dedicated stepping or scanning mobility measurements. For example, the Knutson and Whitby design (Knutson and Whitby 1975), originally designed to produce calibration aerosol at large sample flow rates has been adopted for scanning mobility size spectrometers with little modifications. Compact design of mobility spectrometers requires that the DMA samples only as much flow as that analyzed in the sensing volume of the downstream condensation particle counter (CPC). This allows optimizing the DMA size with respect to operational and measurement characteristics of the overall mobility spectrometers.

In this paper, we describe the design of a miniature DMA (mDMA) that addresses some of the drawbacks discussed above. The mDMA was designed specifically for use in hand-held spectrometers to classify the submicrometer size range at low to moderate size resolution, and with penetration efficiencies comparable to those of the Knutson-Whitby DMA. This was accomplished by using a small sample flow rate in the mDMA that matched the aerosol flow rate in the downstream CPC. The transfer function, mobility resolution, and transmission efficiencies of the DMA were experimentally measured for submicrometer aerosol. The results of these measurements are presented and discussed.

2. Design of the Miniature DMA (mDMA)

The cross-sectional view of the mDMA is shown in Figure 1. It has a cylindrical configuration with an outer cylindrical electrode (E) having an inner diameter (d_o) of 2.54 cm (1.0 inch), and an inner rod (D) with an outer diameter (d_i) of 1.778 cm (0.7 inch). The outer and inner electrodes are concentrically aligned with each other and the space between them forms the classification zone of the mDMA. A large part of the inner electrode rod is hollowed to reduce its weight. Sampled aerosol enters at the center of inlet (A) and subsequently splits into six small channels (diameter of 0.794 mm or 1/32 inch) evenly spaced along the circumference of the flow splitter (B). After passing through the annular chamber between the flow splitter and the top expanded portion of outer cylindrical electrode, the aerosol enters the classification zone through a narrow annular slit located on the outer electrode. Clean sheath flow enters the DMA through a channel in the side of the inlet and flows through 12 holes (diameter of 1.588 mm or 1/16 inch) on the flow splitter. These 12 holes were evenly spaced and staggered with the six channels for the aerosol flow. The sheath flow then enters the classification zone after passing through a flow laminarizer (C), which has 230 evenly distributed small holes (diameter of 0.508 mm or 0.02 inch) to help distribute and create a laminar sheath flow. The sheath flow exiting the flow laminarizer travels 5.588 mm before entering the classification zone of the DMA, which allows uniform circumferential flow distribution obtained at the design aerosol and sheath flow rates. This was qualitatively confirmed with flow visualization using smoke, which revealed uniformly

distributed (azimuthally) laminar flow (see Figure S1 in SI). The flow laminarizer is made of Delrin® and it also serves as an electrical insulator between the flow splitter and the inner rod. The classification zone has a length of 2.54 cm (1.0 inch). The classified aerosol exits the classification zone by entering the flow channels in the inner rod, and subsequently exits the DMA from the center of the outlet (G) part. The aerosol exit flow channels located in the inner rod oriented at an angle of 60° with respect to the longitudinal axis of the central electrode. The detailed configuration of these channels is shown in Figure S2 in SI. Excess flow exits the mDMA from two opposite outlet ports on G after passing through 48 small holes (diameter of 0.794 mm or 1/32 inch) on the outlet insulator (F). Outlet insulator is made of Delrin® and also serves as an electrical insulator. The 48 holes on the outlet insulator and the symmetrically placed outlet ports are designed to help ensure uniform flow in the classification zone.

For a DMA operated under a fixed sheath flow rate, the largest classifiable particle diameter depends on the highest voltage that can be applied on the central electrode of the DMA at a given sheath flow. This voltage limit is normally set to avoid sparking caused by electrical breakdown of gas at high electrical field strength. For a DMA of cylindrical configuration, the highest electrical field strength is at the surface of the central electrode, and the breakdown strength (E_b, unit in KV/cm) can be calculated by Equation (1) (White 1963):

$$E_b = 30 + 12.7 d_i^{-0.5} \quad (1)$$

where, d_i (in cm) is the outer diameter of the central electrode. Using Equation (1), the breakdown strength of the electrical field for the mDMA was found to be 39.5 KV/cm, which is higher than that of the TSI 3081 and 3085 DMAs (39.3 KV/cm).. In practice, the breakdown strength could be much lower than the value calculated from Equation (1), mainly due to the intensified electrical field at the edges of the aerosol entrance and exit slits, the imperfections in electrode alignment or surface finish during fabrication, or the presence of excess moisture or volatile species in the sampled aerosol. Most commercial DMAs are designed not to exceed a maximum electrical field strength (E_{max}) of approximately 15 KV/cm. Using this same limit, the maximum allowable voltage for the mDMA would be 4.8 KV. However, we have been able to operate the mDMA safely at higher voltages up to 6.3 KV (corresponding to E_{max} of 20 KV/cm). The smallest classifiable electrical mobility can then be calculated by,

$$Z^*_{p,\min} = \frac{Q_{sh}}{\pi L d_i E_{\max}} \quad (2)$$

where, Q_{sh} is the sheath flow rate, and L is the length of the classification zone. The largest measurable particle diameter for the mDMA can then be derived using the smallest classifiable electrical mobility for singly charged particles. Figure 2 shows the largest classifiable size (left y-axis) and the theoretical mobility resolution (right y-axis, defined and discussed in Section 4.5) as a function of sheath flow in the DMA.

As shown in Figure 2, with an E_{max} of 20 KV/cm for the mDMA (a factor of ~2 lower than the value used above of 39.5KV/cm), the largest classifiable particle diameter is 921 nm and 515 nm at 0.2 L/min and 0.4 L/min sheath flow rate, respectively. Although the lower sheath flow rate leads to a larger upper size limit of the DMA, it results in a lower mobility resolution of the DMA if the aerosol flow rate remains the same. For a DMA operating in a closed-loop sheath flow, its theoretical mobility resolution for non-diffusive particles is a function of the ratio of its sheath flow rate to its aerosol flow rate, and it is also plotted in Figure 2 for the mDMA operating at a 0.05 L/min aerosol flow rate. Considering both the upper size limit and mobility resolution, the mDMA was designed and evaluated at 0.2 L/min and 0.4 L/min sheath flow rates with a fixed aerosol flow rate of 0.05 L/min in this study. At these operating flow rates, the mDMA covers a large size range below 1 μm and provides a reasonable mobility resolution for personal exposure monitoring and mobile measurement applications.

Overall, the parts in the mDMA can be fabricated at reasonably low cost and they are easy to assemble. The design also allows fabrication of the DMA using additive manufacturing techniques.

3. Experimental Setup

Tandem DMA (TDMA) measurements have been widely used to experimentally obtain the transfer function of a DMA (Stolzenburg 1988; Stolzenburg and McMurry 2008), which characterizes accuracy, precision, and transmission efficiency of the DMA. Ideally, two identical DMA units must be used in the TDMA measurements. A classifying first DMA with a known transfer function has also been used to measure the unknown transfer function of the second DMA (Birmili et al. 1997; Li et al. 2006; Stolzenburg 1988; Stolzenburg and McMurry 2008; Stratmann et al. 1997). In our experimental setup, using two identical mDMAs presented several challenges in maintaining a reliable flow scheme over extended period of time. This was mainly due to significantly low aerosol flow rate (0.05 L/min) in the mDMA. Therefore, we used the first classifying DMA with a known transfer function to probe the transfer function of the test mDMA. The first DMA was operated at a much higher mobility resolution (compared to that of mDMA) to minimize measurement uncertainties.

The experimental setup for TDMA measurements is shown in Figure 3. Both silver nanoparticles (smaller than 50 nm in diameter) and ammonium sulfate particles (50 nm and larger) were used in the experiment. For silver nanoparticles, the test aerosol was produced using a tube furnace as an evaporation-condensation particle generator. A pneumatic atomizer (Model 3076; TSI Inc., Shoreview MN) was used to atomize an aqueous solution of ammonium sulfate to produce the ammonium sulfate test particles after passing the aerosol through a diffusion dryer. The concentration of the aqueous solution of ammonium sulfate was controlled so that the geometric mean diameter of the polydisperse aerosol generated from the atomizer was below 50 nm. This was to minimize the effect of multiply charged particles on the TDMA test. Test aerosols from different aerosol generators were subsequently charge-conditioned using a Kr^{85} neutralizer and then classified in the 1st DMA (Model 3081 for 200 nm particles and 3085 for particles of the other sizes; TSI Inc., Shoreview MN; operating at a 20:1 sheath-to-aerosol flow ratio) to provide monodisperse

test particles. An Electrostatic Classifier (Model 3080; TSI Inc., Shoreview MN) controlled the sheath flow rate and voltage for the 1st DMA. An Ultrafine Condensation Particle Counter (UCPC, Model 3025A, TSI Inc., Shoreview MN) continuously monitored the concentration of particles exiting the 1st DMA at a flow rate of 0.3 L/min. The rest of the size-classified aerosol then entered a three-way valve at a flow rate of 0.05 L/min so that the concentration of particles upstream and downstream of the mDMA was measured by switching the three-way valve and directing the aerosol to a CPC. The particle loss in the two flow paths downstream of the three-way valve was measured and found to be identical. The CPC (Kanomax USA Inc., Andover, NJ) was specifically designed to operate at 0.05 L/min, which had a counting efficiency of 50% at 10 nm (Qi et al. 2011). As mentioned earlier, the mDMA was evaluated at an aerosol sampling flow rate of 0.05 L/min and sheath flow rates of 0.2 L/min and 0.4 L/min. The sheath flow for the mDMA was operated in a closed loop, and it was controlled and monitored by a modified electrostatic classifier set up (Model 3080, TSI Inc.).

When conducting the TDMA measurements, the first DMA was operated at a fixed sheath flow rate and its electrode voltage was set to correspond to desired test particle diameter. Two DC power supplies stepped through the entire voltage range for the mDMA under test. For improved accuracy, a DC power supply (Model GPR-30H10D, Good Will Instrument Co., Ltd, New Taipei City, Taiwan) applied a voltage between 0 to 300 V. This applied voltage was simultaneously monitored by using a multimeter (Fluke 111 True RMS; Fluke Corporation, Everett WA). A high-voltage power supply (Bertan Model 206B-10R, Spellman High Voltage Electronics Corporation, Hauppauge NY) provided the voltage above 300 V. This voltage was monitored using the multimeter through a HV probe (Model Fluke 80K-6; Fluke Corporation, Everett WA). Stepping through a series of voltages, an experimental TDMA curve was obtained by normalizing the particle concentrations measured by the same CPC downstream (N_2) and upstream (N_1) of the mDMA at a given voltage. Identical lengths of tubing (and the flow rate) established the flow paths for the measurement of N_1 and N_2, such that particle losses in the transport tubing (without the DMA) of both flow paths were identical and did not introduce error in the measurement of N_2/N_1. The particle concentration downstream of the first DMA was monitored using the UCPC during the TDMA measurements to account for any concentration fluctuation of the test aerosol during the measurement of N_1 and N_2 ($N_{3,1}$ and $N_{3,2}$ corresponding to N_1 and N_2, respectively).

4. Results and Discussions

4.1 Data deconvolution

Test particles were classified in the first DMA with a 20:1 sheath to aerosol flow rate ratio. Voltage applied on the mDMA was varied and the particle number concentration upstream (N_1) and downstream (N_2) of the mDMA were recorded by the CPC. The distribution of ratio N_2 to N_1 is then given by (Li et al. 2006),

$$\frac{N_2(V_1,V_2)/N_{3,2}}{N_1(V_1)/N_{3,1}}=\frac{\int_0^\infty \Omega_1(Z_p,V_1)\Omega_2(Z_p,V_2,L_{\text{eff}},f_v,f_\sigma)dZ_p}{\int_0^\infty \Omega_1(Z_p,V_1)dZ_p} \quad (3)$$

Where, V_1 is voltage applied on the first DMA, V_2 is voltage applied on the mDMA, Ω_1 is transfer function of the first DMA, and Ω_2 is transfer function of the mDMA. A deconvolution scheme involving a nonlinear least-square fitting of the diffusional transfer function model (Stolzenburg and McMurry 2008) was used to retrieve the transfer function of the mDMA. Three parameters L_{eff}, f_v, and f_σ were used as fitting parameters to reconcile the experimentally measured convoluted transfer function data with that predicted from theory using the Stolzenburg model. The factor L_{eff} accounts for transmission efficiency (described by Equation (5)–(7)), f_v accounts for shift in the voltage, and f_σ accounts for broadening of the transfer function in addition to diffusion by non-ideal conditions in the instrument.

Figure 4 shows the TDMA curves obtained experimentally for 20 nm and 200 nm test particles at two sheath flow rate of 0.2 L/min and 0.4 L/min, respectively. The error bars shown in Figure 4 represent the propagated measurement uncertainty calculated from multiple measurements of particle concentrations for obtaining each data point (i.e. N_1, N_2, $N_{3,1}$ and $N_{3,2}$). The uncertainty for each measurement of aerosol concentration represents the standard deviation of measurements over a period of 10 s or more. The propagated measurement uncertainty was calculated following the procedure described by Qi and Kulkarni (2012).

The first DMA is set to classify particles at centroid mobility of Z^*_{p1}. $Z^*_{p1,2}$ in Figure 4 is the centroid electrical mobility of the test particles classified by the first DMA under temperature and pressure conditions inside the mDMA. Assuming particle diameter is fixed during the TDMA measurements, it was obtained with the knowledge of the centroid electrical mobility of the first DMA (Z^*_{p1}) after taking into account the slight changes in temperature and pressure between the two DMAs. Particle's centroid electrical mobility in the mDMA (Z^*_{p2}), corresponding to the applied voltage on the central electrode of the mDMA (V_2), can be obtained using the following equation:

$$Z^*_{p2}=\frac{Q_{sh}}{2\pi V_2 L}\ln\left(\frac{d_o}{d_i}\right) \quad (4)$$

The first DMA used in our setup is a widely used commercial units whose transfer function has been very well characterized (Chen et al. 1998; Jiang et al. 2011; Stolzenburg 1988). With the knowledge of the transfer function of the first DMA and the experimental TDMA curve, the transfer function of the mDMA was obtained through a deconvolution algorithm similar to the one used by Stolzenburg (1988). In this approach, the diffusion theory was used to describe the diffusive broadening of the DMA transfer function, and three fit parameters were used to account for the difference between the experimental data and

theoretical prediction. The three free fit parameters include: f_v, which accounts for the difference between the calculated centroid electrical mobility and the actual centroid electrical mobility for the mDMA; f_σ, which accounts for the additional broadening resulting from nonideal conditions in the mDMA; and η, which accounts for the particle penetration through the entrance and the exit regions of the mDMA.

Details of this approach were described by Stolzenburg (1988) and have been used by several studies to measure the transfer function of the DMA (Birmili et al. 1997; Chen et al. 1998; Fissan et al. 1998; Karlsson and Martinsson 2003; Li et al. 2006; Stolzenburg and McMurry 2008)...

We used a diffusional deposition model to parameterize the transmission efficiency η of the mDMA, following similar approach by Jiang et al. (2011). The transmission efficiency $\eta(d_p)$ was parameterized as a function of effective column length (L_{eff}) of the mDMA using the equations given by Cheng (2011) as:

$$\eta(\mathrm{d_p})=0.819\exp(-3.66\mu)+0.0975\exp(-22.3\mu)+0.0325\exp(-57.0\mu)+0.0154\exp(-107.6\mu) \quad \text{for } \mu>0.02 \tag{5}$$

$$\eta(\mathrm{d_p})=1.0-2.56\mu^{2/3}+1.2\mu+0.1767\mu^{4/3} \text{ for } \mu \leq 0.02 \tag{6}$$

where, d_p is the mobility diameter of the particle, and μ is the dimensionless deposition parameter defined as:

$$\mu=\frac{\pi D L_{\mathrm{eff}}}{Q_a} \tag{7}$$

where, Q_a is the aerosol flow rate in the mDMA; D is the diffusion coefficient of particles with diameter d_p.

The three empirical fit parameters f_v, f_σ, and L_{eff} can be obtained by using a least squares fitting method which aims to reconcile the difference between the curves obtained experimentally and those predicted from the diffusion theory. One set values of the three parameters f_v, f_σ, and L_{eff} were obtained for each set of TDMA measurement using the least squares fitting described earlier. Because the transfer function model was most sensitive to f_v, it was treated as a free parameter in the least square fitting process for each set of TDMA data, while assuming a constant L_{eff} and f_σ. Figure 5 shows values of f_v obtained from the least squares solution with a L_{eff} of 1.85 m for all cases, and f_σ = 1.0 for Q_{sh}= 0.2 L/min and f_σ =1.3 for Q_{sh} =0.4 L/min, respectively. Also shown in Figure 4 are the convoluted TDMA curves predicted using the transfer functions based on the fitted parameters obtained through the least squares fitting of the experimental data. These curves show good agreement,

indicating that the theoretical transfer function model used adequately explains the experimentally measured TDMA curves.

The constant value of fitted L_{eff} across all measured data suggests that the transmission loss in the mDMA could possibly be attributed to the aerosol flow in the entrance and exit regions. The fitting process was relatively insensitive to the value of f_σ, particularly at the smaller sheath flows. For particles tested in this study between 20 nm and 200 nm, the additional broadening of the transfer function represented by f_σ was insignificant compared to the diffusional broadening at low sheath flow rate, and increased slightly at higher sheath flow rate (0.4 L/min)..

4.2 Mobility Classification Accuracy of the mDMA

The factor f_v accounts for the difference between the theoretical centroid electrical mobility and the experimentally measured centroid electrical mobility (derived from TDMA measurements) of the mDMA. The measured centroid electrical mobility of the mDMA transfer function is dependent on the known transfer function of the first DMA. Since the first DMA was calibrated with NIST traceable particle size standards, it was assumed that it provided classified aerosol with known reference centroid mobility (Z_{p1}^*). Therefore f_v obtained from the TDMA measurements, reflects the accuracy of mobility classification (and implied size classification accuracy) of the mDMA. The fitted f_v for each set of experimental TDMA curve is plotted in Figure 5; all values are close to 1.0 (mean was 1.015 and 0.953 at sheath flow rate of 0.2 L/min and 0.4 L/min, respectively). This demonstrates good overall mobility (or size) classification accuracy of the mDMA. It should be noted that the f_v values obtained reflect both the accuracy of the mDMA transfer function and additional sources of error from variations in sheath flow rate and mDMA geometry.

4.3 Transfer function of the mDMA

Figure 6 shows theoretical and experimental transfer functions of the mDMA for 20 nm and 200 nm particles at two sheath flow rate of 0.2 L/min and 0.4 L/min. The theoretical transfer function was calculated using f_v=1, f_σ=1, and L_{eff}=0; whereas the experimental transfer function was obtained using the fitted values for the three parameters. As expected, the transfer functions for 20 nm particles are Gaussian-shaped due to diffusional broadening, and the peak transmission efficiency, or peak height, is 0.421 and 0.335 for 0.2 L/min and 0.4 L/min sheath flow rate, respectively. The corresponding theoretical value (using the Stolzenburg transfer function) for peak height is 0.700 and 0.630 at 0.2 and 0.4 L/min sheath flow rates. The reduced peak transmission efficiency of the mDMA is mainly attributed to additional losses in the entrance and exit regions of the mDMA (parameterized by L_{eff}). The diffusional loss for 200 nm particles is insignificant, resulting in a negligible difference between the experimental and theoretical transfer functions (not shown in Figure 6 (b)). As expected, the transfer function for 200 nm particles shows minimal diffusional broadening and is triangular, with the maximum transmission efficiency being 0.919 and 0.900 at 0.2 L/min and 0.4 L/min sheath flow rate, respectively.

The transmission efficiency of the mDMA can be obtained from the area under the transfer function deconvoluted from the experimental data and derived from the ideal diffusion

theory (Mei et al. 2011). As discussed earlier, the mDMA was designed to operate at a sheath flow rate of 0.2 L/min or 0.4 L/min to have an extended upper size limits as shown in Figure 2. The diffusional loss inside the mDMA was accounted for using the laminar diffusional deposition model for cylindrical tubes parameterized by the effective column length L_{eff}. A constant L_{eff} of 1.85 m was obtained for the mDMA by fitting all of the experimental data. The corresponding transmission efficiency was obtained from the ratio of the areas under each pair of the transfer functions. The results of the transmission efficiency for the mDMA are plotted in Figure 7. The transmission efficiency is 93.3% for 100 nm particles and 57.7% for 20 nm particles. However, it reduces to 15.5% for 10 nm particles.

For comparison, the transmission efficiency was also obtained for two other DMAs and are shown in Figure 7. The L_{eff} for the TSI 3085 nano DMA was 3.64 m and was obtained from Jiang et al. (2011), who used the same parameterization as in Equations (5) – (7). Using parameterization of Soderholm (1979), Reineking and Porstendörfer (1986) obtained a L_{eff} value of 13 m for the TSI 3071 long DMA. Using our parameterization (Equation (5) – (7)) on the TDMA measurements of Reineking and Porstendörfer (1986), we obtained L_{eff} of 12.1 m for the TSI 3071 DMA. For both the TSI 3071 and 3085 DMAs, the results were obtained for an aerosol flow rate of 0.05 L/min as well as 1.5 L/min.

As shown in Figure 7, when running at an aerosol flow rate of 0.05 L/min, the mDMA provides higher transmission efficiency than the TSI 3071 and 3085 DMAs. This was expected due to the smaller value of L_{eff} for the mDMA, and it also validates the optimal design of the entrance and exit regions of the mDMA for low flow rates. An aerosol flow rate of about 1.5 L/min is more commonly used in the two TSI DMAs and their transmission efficiencies under this flow rate is higher than that of the mDMA operated at a 0.05 L/min aerosol flow rate. This was also expected due to the lower particle loss at a higher flow rate. However, the two TSI DMAs would then need to be operated at a sheath flow rate of 12.0 L/min to maintain a sheath to aerosol flow ratio of 8, resulting in an upper size limit of only 75 nm for the TSI 3085 DMA and 279 nm for the TSI 3071 DMA, assuming a 10 KV maximum voltage. The mDMA operated at an aerosol flow rate 0.05 L/min and a sheath flow rate of 0.4 L/min would provide the same sheath-to-aerosol flow ratio while extending the upper size limit to 515 nm at its designed E_{max} of 20 KV/cm. The transmission efficiency was plotted for a particle diameter up to the respective upper size limit for each case in Figure 7.

4.4 Mobility resolution of the mDMA

As mentioned earlier and illustrated in Figure 2, the theoretical mobility resolution of a DMA for non-diffusive particles is proportional to the ratio of the sheath to aerosol flow ratio. The actual resolution deteriorates mainly due to the Brownian diffusion of particles, and additional broadening resulting from non-ideal flow and electrical field conditions in the DMA. Mobility resolution can be defined as the inverse of the normalized full-width at half-maximum (FWHM) of transfer function (Flagan 1999):

$$R=\frac{Z_p}{\Delta Z_{p,fwhm}} \quad (8)$$

where $\Delta Z_{p,fwhm}$ is full width of the transfer function at half the maximum height. Using the theoretical and experimental transfer functions, mobility resolution was calculated at different particle diameters for all the DMAs used in this study and are shown in Figure 8. Figure 8(a) shows resolution of mDMA at two sheath flow rates; symbols show the resolution derived from the experimentally measured transfer function. For comparison, the sizing resolutions calculated from the transfer functions derived from the ideal diffusion theory for the mDMA were plotted using two curves in the figure. Their deviation from the theoretical limit (horizontal dotted lines) at the mobility resolution of 4 and 8 for the sheath flow rate of 0.2 L/min and 0.4 L/min represent the deterioration of sizing resolution due to the diffusional broadening effect; and their respective deviation from the filled and open circle symbols represent the deterioration of sizing resolution due to non-ideal conditions in the mDMA. Overall, the results in Figure 8(a) reveal that the non-ideal conditions in the mDMA lead to minor deterioration of its sizing resolution.

Mobility resolution of mDMA, TSI 3071 and 3085 DMAs derived from ideal diffusion theory with their respective fitted parameters are shown in Figure 8(b). Figure 8(b) compares the actual mobility resolution of the mDMA and that of the TSI 3071 and 3085 DMAs under the same sheath to aerosol flow ratio of 8. For the two TSI DMAs, aerosol flow rates of 0.05 L/min and 1.5 L/min were both considered. An average value of the fitted factor f_σ was 1.01 for both the TSI 3071 (Stolzenburg 1988) and 3085 (Jiang et al. 2011) DMAs. This mean value was used together with the aforementioned L_{eff} values for the two TSI DMAs to calculate their transfer functions and subsequently, mobility resolutions. As shown in the figure, the mDMA provides resolutions similar to those provided by the TSI 3085 DMA when both are operated at a 0.05 L/min aerosol flow rate; and they are both considerably better than the TSI 3071 DMA under this aerosol flow rate. The two TSI DMAs provides better resolution when operated at a 1.5 L/min aerosol flow rate compared to the mDMA operated at the 0.05 L/min aerosol flow rate. This was expected due to the lower particle loss and diffusional broadening at a higher aerosol flow rate. As explained earlier, the lower aerosol flow rate designed for the mDMA was chosen to extend its upper size classification limit. The tradeoff is reduced transmission efficiency and size resolution..

5. Conclusions

The mDMA was designed to classify submicron particles for personal exposure monitoring and mobile measurements. The design specifically addresses the need to use very low aerosol sample flow rates needed to achieve particle size classification over a wide submicrometer size range in a compact instrument. The design allows fabrication of a low-cost, compact DMA that is easy to assemble. The performance of the mDMA was characterized using a tandem DMA (TDMA) technique operated at an aerosol flow rate of 0.05 L/min and a sheath flow rate of 0.2 L/min or 0.4 L/min. The transfer function of the mDMA was described using Stolzenburg's model. The experimentally measured transfer

function shows good agreement with the theoretical values derived using Stolzenburg's model of the transfer function. The transmission efficiency is adequate and comparable to other DMA designs for particles in the range 10–1000 nm. The mobility resolution is comparable to that of the TSI 3085 nanoDMA at the same aerosol flow rates. The design features and performance make the mDMA suitable for compact field portable mobility size spectrometers for submicrometer aerosol measurement.

Supplementary Material

Refer to Web version on PubMed Central for supplementary material.

Acknowledgments

Authors would like to thank the anonymous reviewers for their insightful comments and Gregory Deye of NIOSH for helping with DMA flow visualization.

References

Birmili W, Stratmann F, Wiedensohler A. Design of a Dma-Based Size Spectrometer for Large Particle Size. J. Aerosol Sci. 1999; 30:549–553.

Birmili W, Stratmann F, Wiedensohler A, Covert D, Russell LM, Berg O. Determination of Differential Mobility Analyzer Transfer Functions Using Identical Instruments in Series. Aerosol Sci. Technol. 1997; 27:215–223.

Brunelli NA, Flagan RC, Giapis KP. Radial Differential Mobility Analyzer for One Nanometer Particle Classification. Aerosol Sci. Technol. 2009; 43:53–59.

Chen DR, Pui DYH, Hummes D, Fissan H, Quant FR, Sem GJ. Design and Evaluation of a Nanometer Aerosol Differential Mobility Analyzer (Nano-Dma). Journal of Aerosol Science. 1998; 29:497–509.

Cheng, YS. Instruments and Samplers Based on Diffusional Separation. In: Kulkarni, P.; Baron, PA.; Willeke, K., editors. Aerosol Measurement: Principles, Techniques, and Applications. New York, NY: John Wiley and Sons; 2011.

Fissan H, Pöcher A, Neumann S, Boulaud D, Pourprix M. Analytical and Empirical Transfer Functions of a Simplified Spectrometre De Mobilite Electrique Circulaire (Smec) for Nano Particles. Journal of Aerosol Science. 1998; 29:289–293.

Flagan RC. On Differential Mobility Analyzer Resolution. Aerosol Science and Technology. 1999; 30:556–570.

Jiang J, Attoui M, Heim M, Brunelli N, McMurry P, Kasper G, Flagan R, Giapis K, Mouret G. Transfer Functions and Penetrations of Five Differential Mobility Analyzers for Sub-2 Nm Particle Classification. Aerosol science and technology. 2011; 45:480–492.

Karlsson MNA, Martinsson BG. Methods to Measure and Predict the Transfer Function Size Dependence of Individual Dmas. Journal of Aerosol Science. 2003; 34:603–625.

Knutson EO, Whitby KT. Aerosol Classification by Electric Mobility: Apparatus, Theory, and Applications. Journal of Aerosol Science. 1975; 6:443–451.

Li L, Chen D-R, Qi C, Kulkarni PS. A Miniature Disk Electrostatic Aerosol Classifier (Mini-Disk Eac) for Personal Nanoparticle Sizers. Journal Of Aerosol Science. 2009; 40:982–992.

Li WL, Li L, Chen DR. Technical Note: A New Deconvolution Scheme for the Retrieval of True Dma Transfer Function from Tandem Dma Data. Aerosol Sci. Technol. 2006; 40:1052–1057.

Liu BYH, Pui DYH. On the Performance of the Electrical Aerosol Analyzer. J. Aerosol Sci. 1975; 6:249–264.

Mei F, Fu H, Chen D-R. A Cost-Effective Differential Mobility Analyzer (Cdma) for Multiple Dma Column Applications. Journal of aerosol science. 2011; 42:462–473.

Mesbah, B. Le Spectroḿetre DeMobilíte Electrique Circulaire S.M.E.C. Th̃eorie, Performances et Applications-Contamination Contrôĺ ee des Surfaces Granuloḿetrie de l'Áerosol Fin. Paris: Universit´e Paris XII; 1994.

Qi C, Kulkarni P. Unipolar Charging Based, Hand-Held Mobility Spectrometer for Aerosol Size Distribution Measurement. Journal Of Aerosol Science. 2012; 49:32–47.

Qi, C.; Kulkarni, P.; Kato, T.; Fukushima, N. Development of Portable Aerosol Electrical Mobility Spectrometer (Paems) for Aerosol Exposure Measurement. 30th Annual meeting of the American Association for Aerosol Research; Orlando, Florida. 2011.

Reineking A, Porstendörfer J. Measurements of Particle Loss Functions in a Differential Mobility Analyzer (Tsi Model 3071) for Different Flow Rates. Aerosol Sci. Technol. 1986; 5:483–486.

Soderholm S. Analysis of Diffusion Battery Data. Journal of aerosol science. 1979; 10:163–175.

Stolzenburg, MR. Mechanical Engineering. Minneapolis, Minnesota: University of Minnesota; 1988. An Ultrafine Aerosol Size Distribution Measuring System.

Stolzenburg MR, McMurry PH. Equations Governing Single and Tandem Dma Configurations and a New Lognormal Approximation to the Transfer Function. Aerosol Science and Technology. 2008; 42:421–432.

Stratmann F, Kauffeldt T, Hummes D, Fissan H. Differential Electrical Mobility Analysis: A Theoretical Study. Aerosol Sci. Technol. 1997; 26:368–383.

White, HJ. Industrial Electrostatic Precipitation. Massachusetts: Addison-Wesley; 1963.

Winklmayr W, Reischl GP, Lindner AO, Berner A. A New Electromobility Spectrometer for the Measurement of Aerosol Size Distributions in the Size Range from 1 to 1000 Nm. Journal of Aerosol Science. 1991; 22:289–296.

Zhang SH, Akutsu Y, Russell LM, Flagan RC, Seinfeld JH. Radial Differential Mobility Analyzer. Aerosol Science and Technology. 1995; 23:357–372.

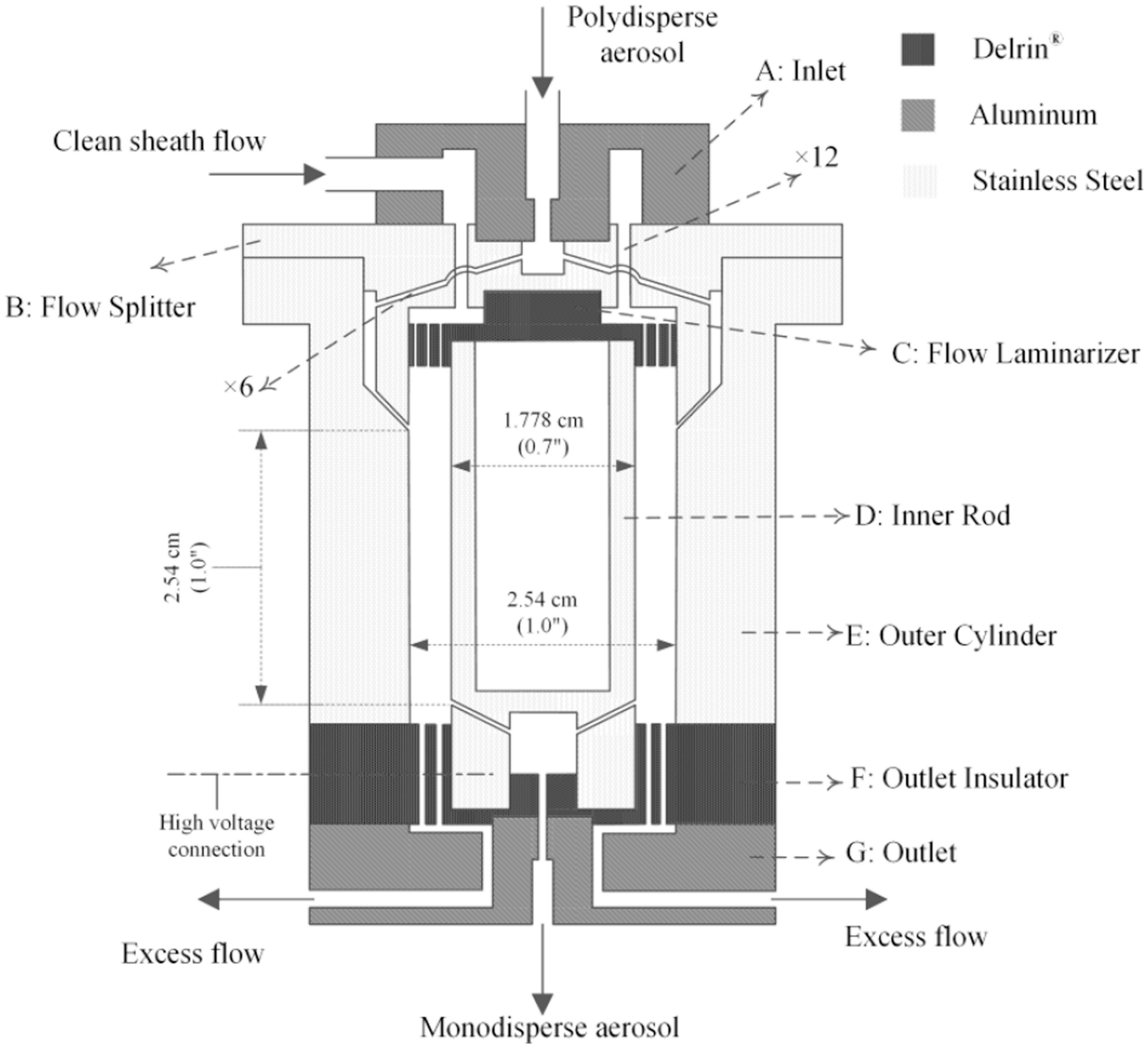

Figure 1.
Schematic diagram of the mDMA

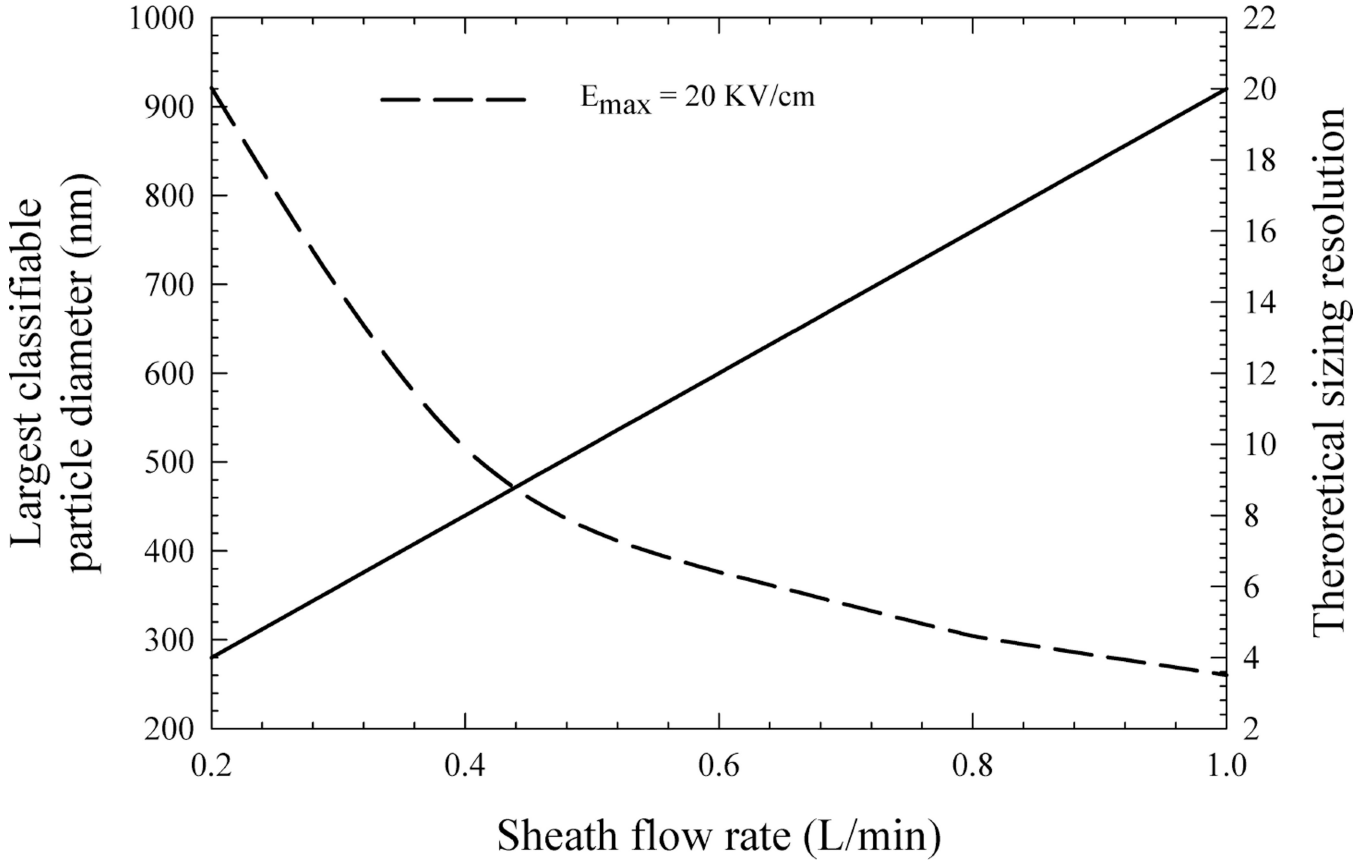

Figure 2.
The largest classifiable particle diameter and the maximum theoretical mobility resolution of the mDMA at different sheath flow rates.

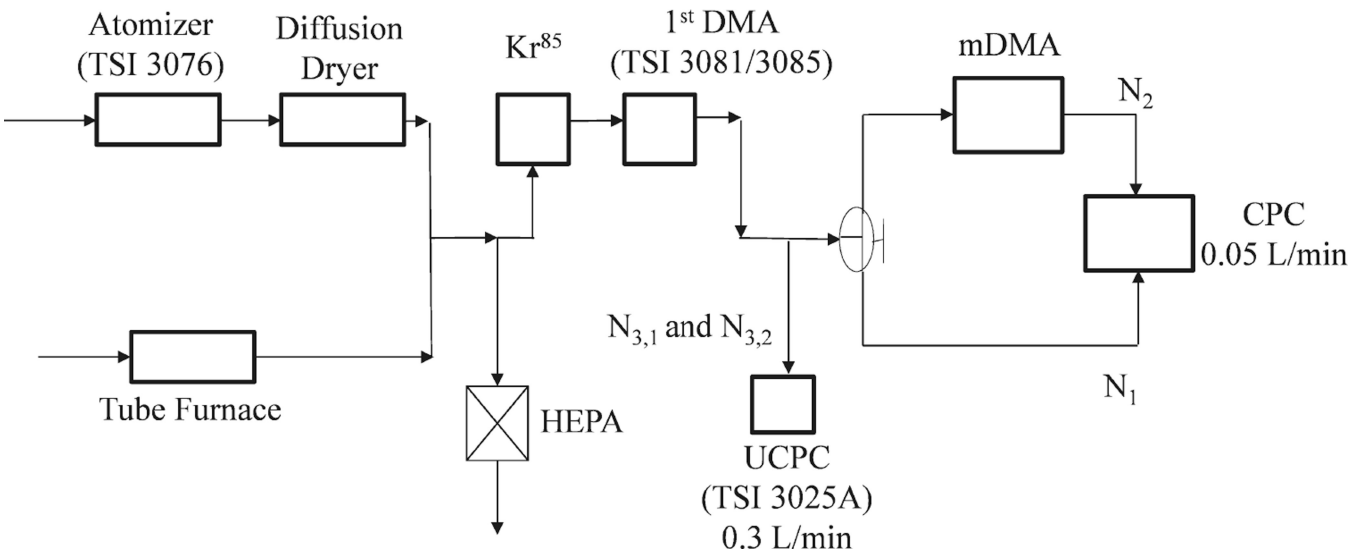

Figure 3.
Schematic diagram of the experimental setup used for the TDMA measurements

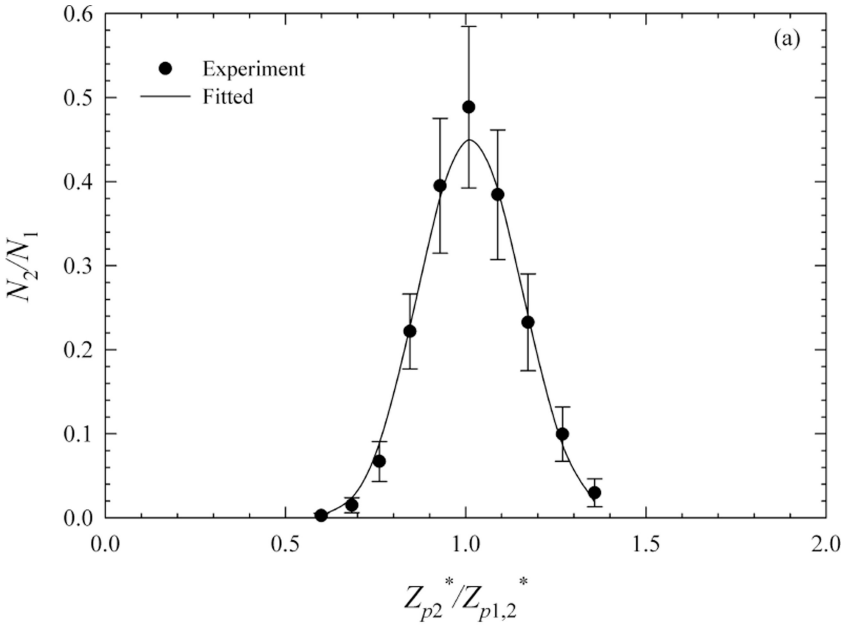

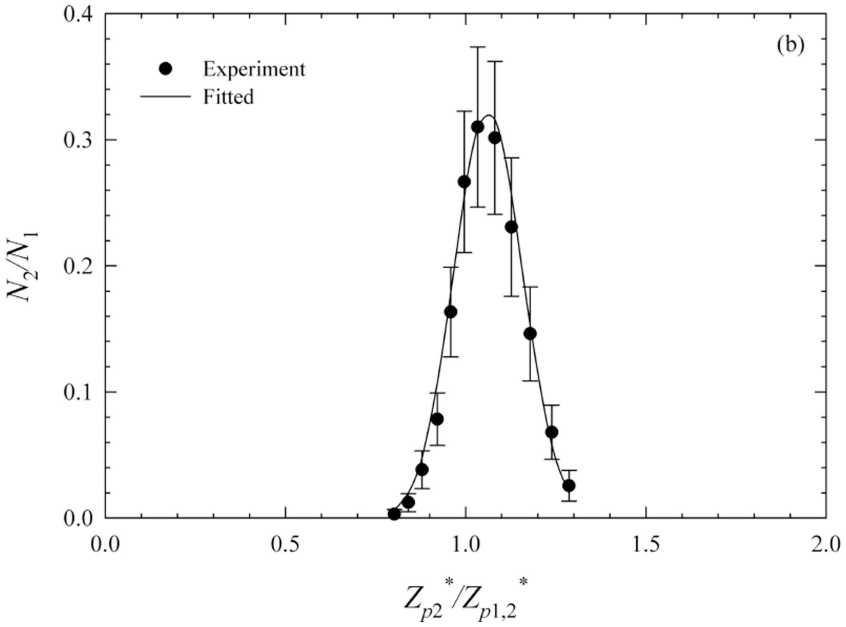

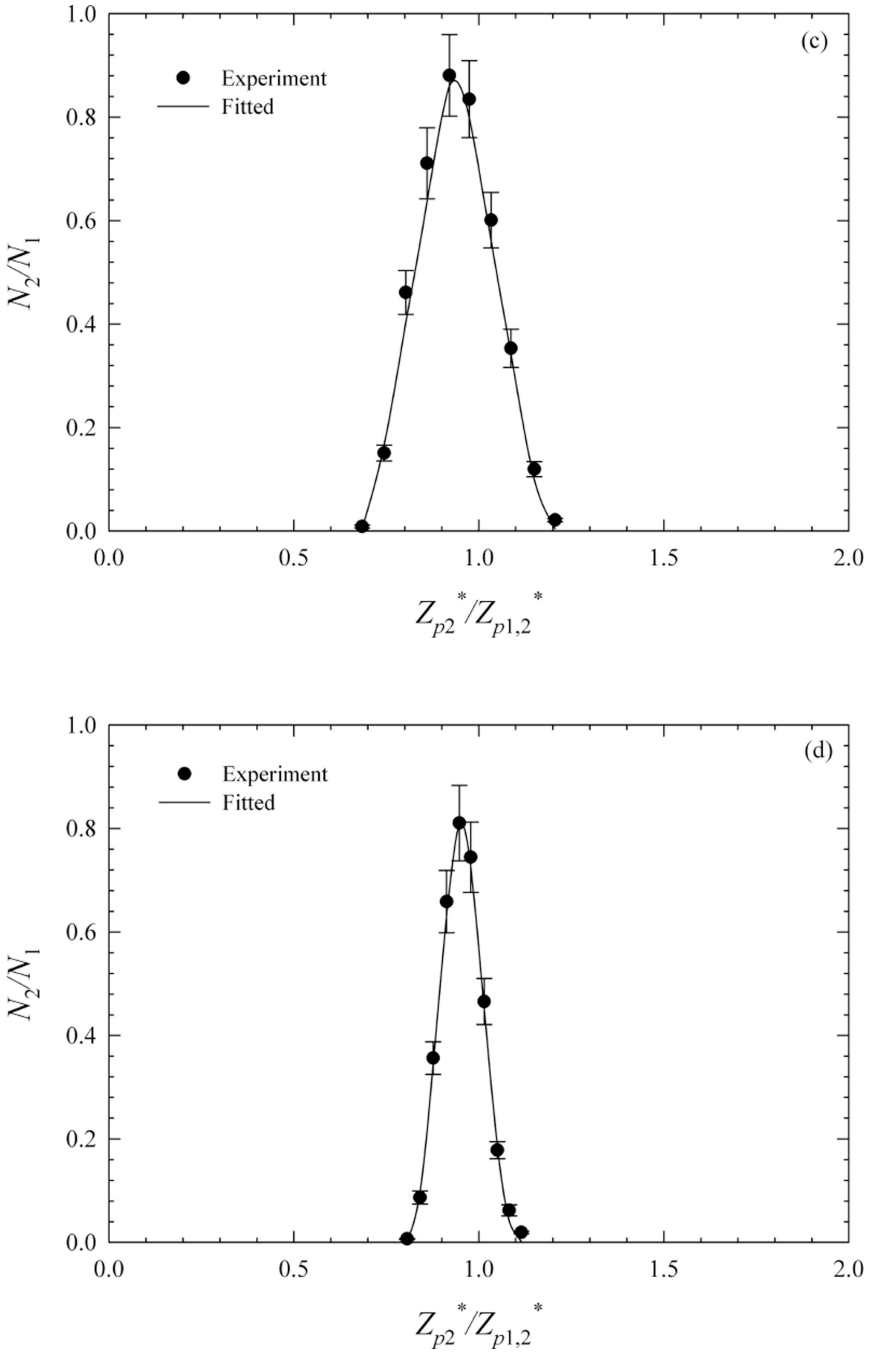

Figure 4.

The comparison of the experimentally measured and fitted theoretically computed TDMA curves of the mDMA for: (a) 20 nm, Q_{sh} = 0.2 L/min; (b) 20 nm, Q_{sh} = 0.4 L/min; (c) 200 nm, Q_{sh} = 0.2 L/min; (d) 200 nm, Q_{sh} = 0.4 L/min.

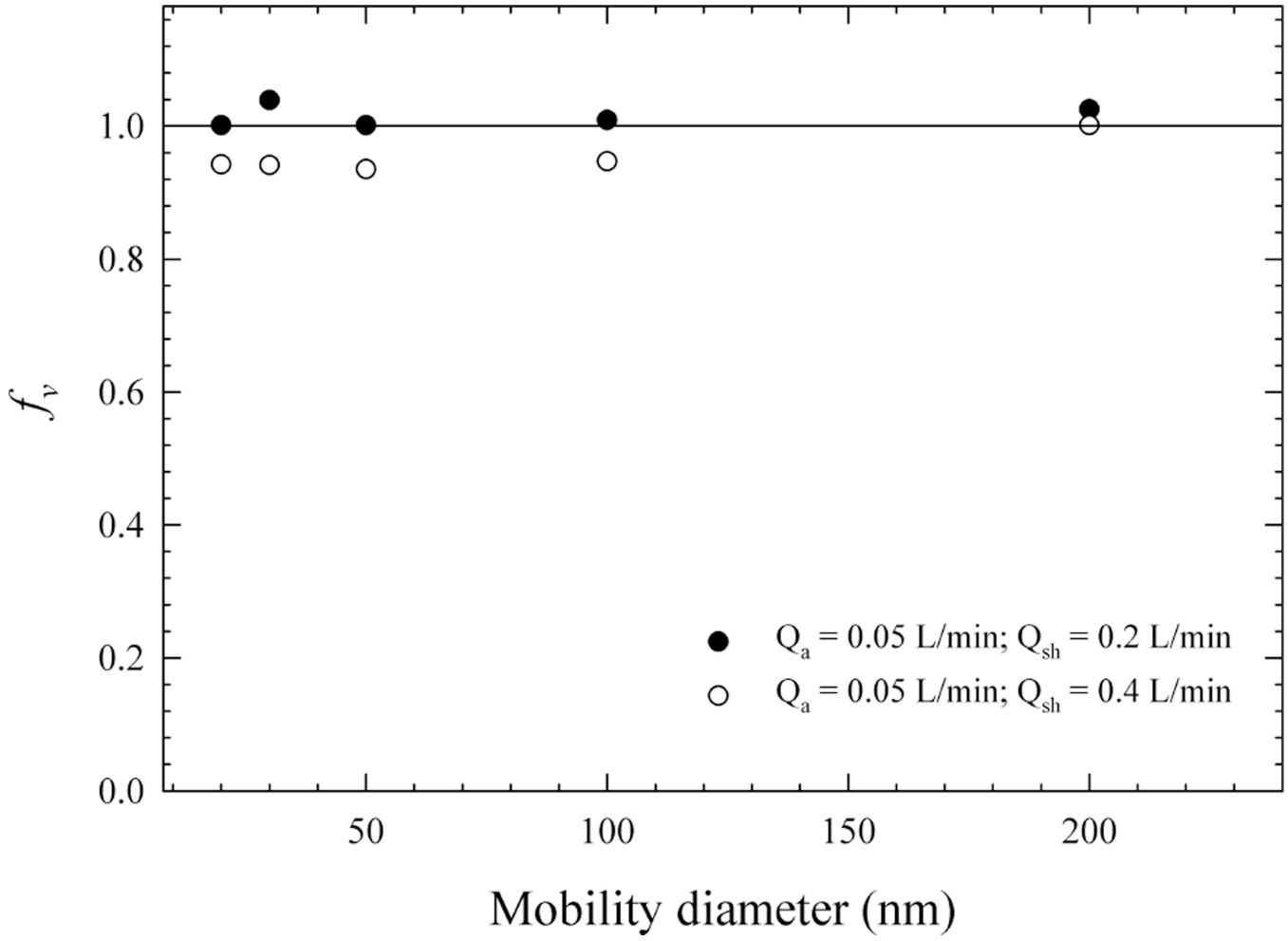

Figure 5.
Variation of fit parameter f_v of the mDMA as a function of mobility diameter.

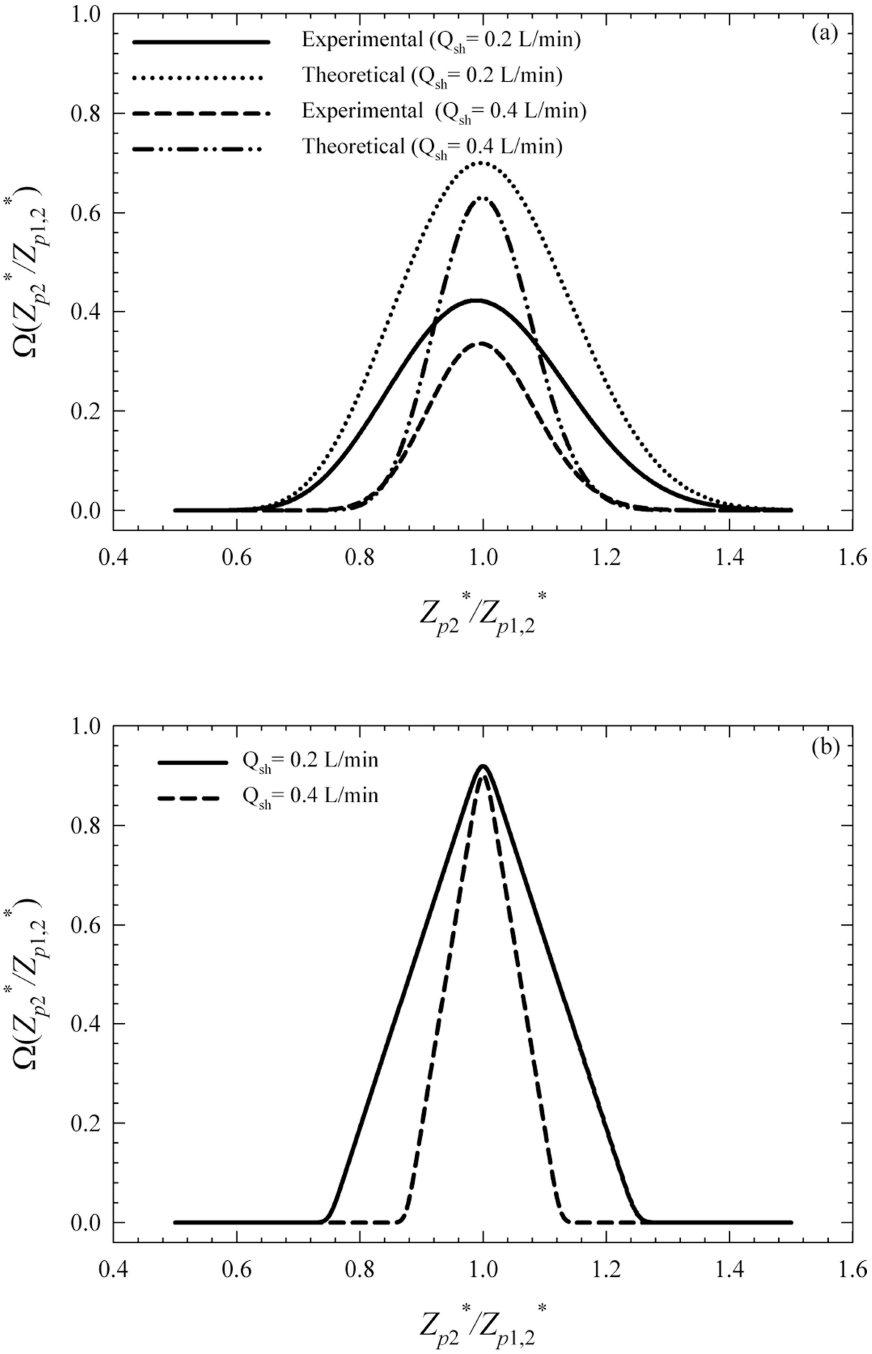

Figure 6.
The transfer function of the mDMA for particles of diameter (a) 20 nm; and (b) 200 nm.

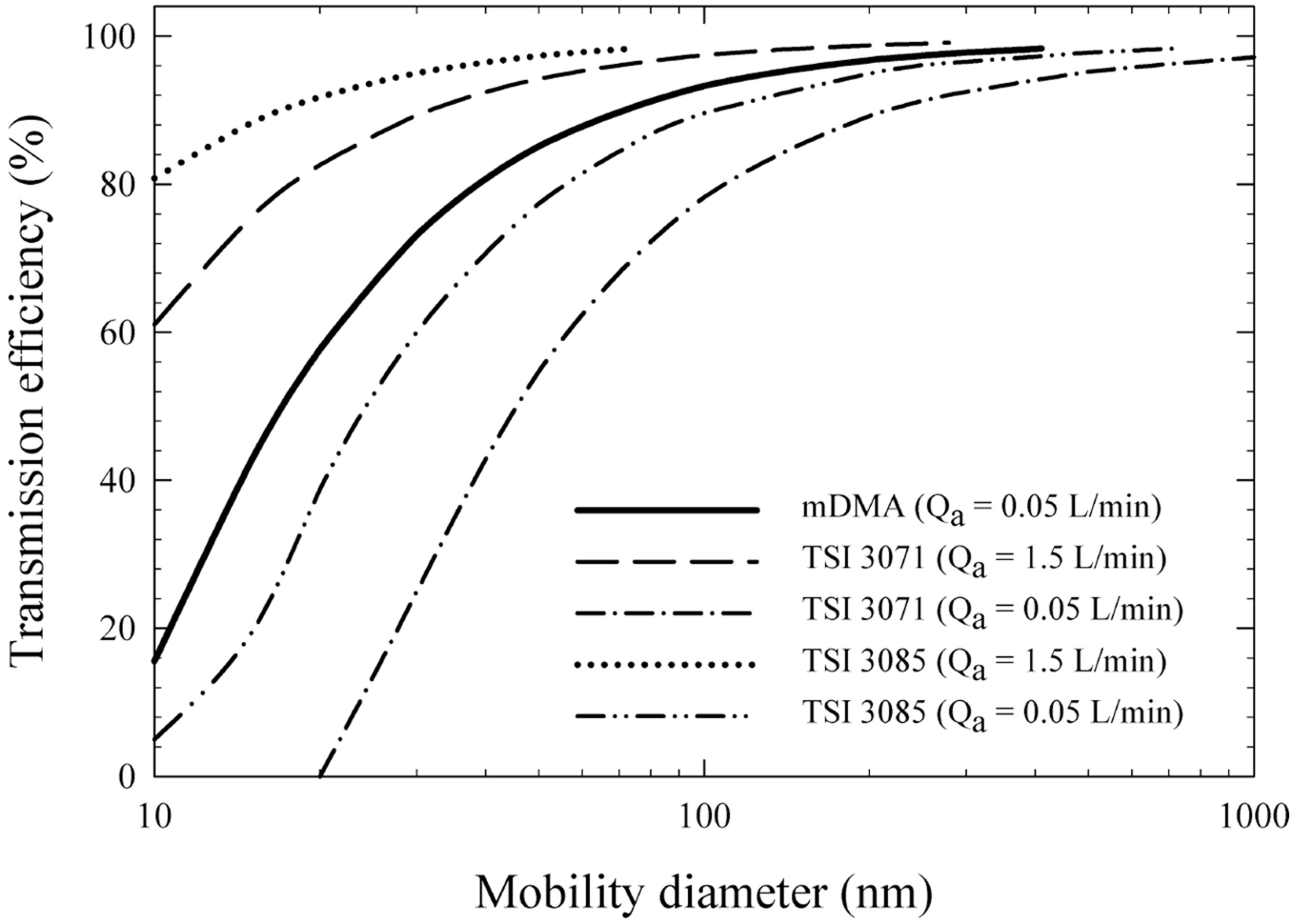

Figure 7.
Comparison of the transmission efficiency of the mDMA with two TSI DMAs.

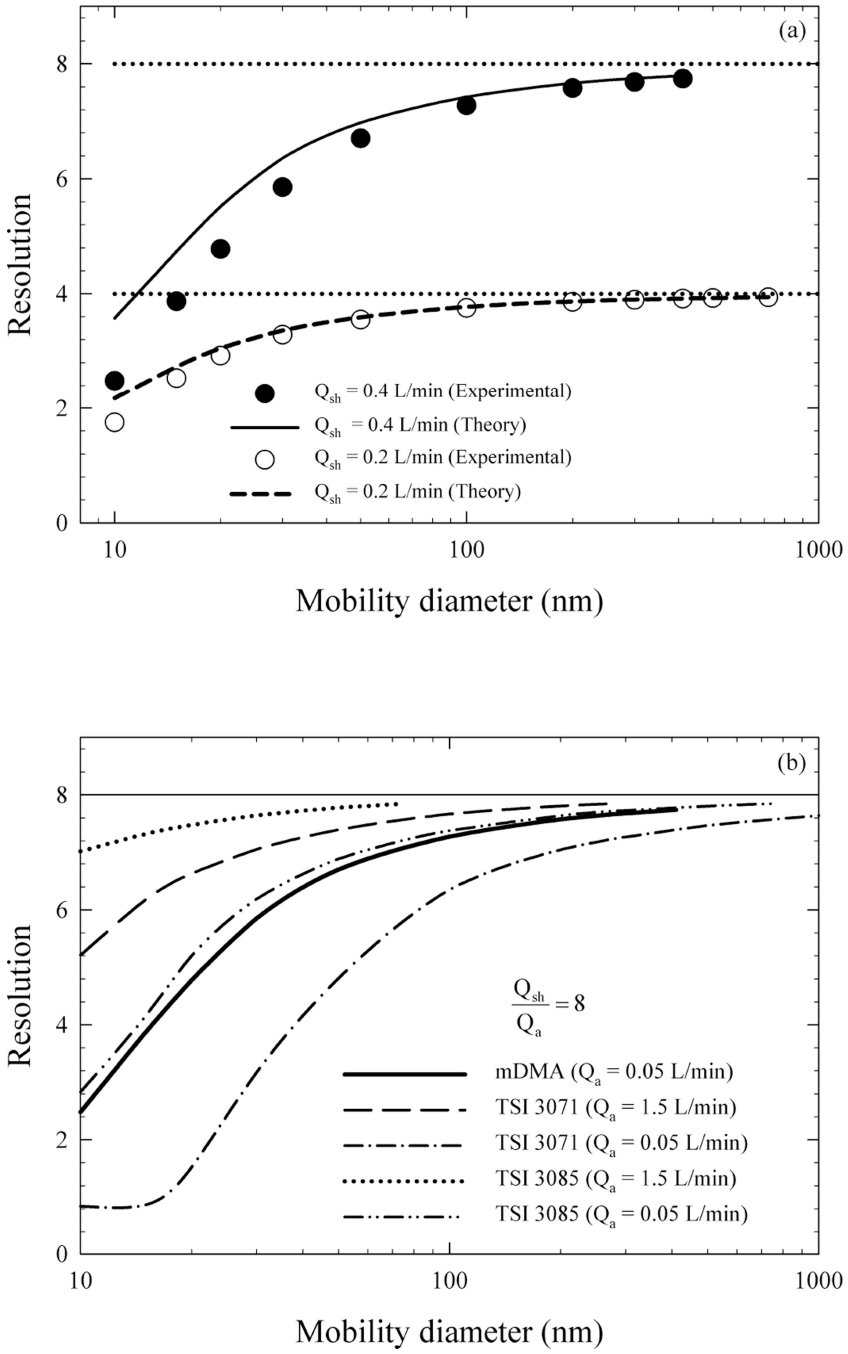

Figure 8.
(a) Mobility resolution of the mDMA; (b) the comparison of the mobility resolution between the mDMA and the TSI DMA 3071 and 3085.